UC Davis

UC Davis Previously Published Works

Title

Pharmacological reactivation of inactive X-linked *Mecp2* in cerebral cortical neurons of living mice.

Permalink

https://escholarship.org/uc/item/3dh8q395

Journal

Proceedings of the National Academy of Sciences of the United States of America, 115(31)

ISSN

0027-8424

Authors

Przanowski, Piotr
Wasko, Urszula
Zheng, Zeming
et al.

Publication Date

2018-07-01

DOI

10.1073/pnas.1803792115

Peer reviewed

eScholarship.org Powered by the California Digital Library
University of California

Pharmacological reactivation of inactive X-linked *Mecp2* in cerebral cortical neurons of living mice

Piotr Przanowski[a], Urszula Wasko[a], Zeming Zheng[a], Jun Yu[b], Robyn Sherman[a], Lihua Julie Zhu[b,c], Michael J. McConnell[a,d], Jogender Tushir-Singh[a], Michael R. Green[b,e,1], and Sanchita Bhatnagar[a,d,1]

[a]Department of Biochemistry and Molecular Genetics, University of Virginia School of Medicine, Charlottesville, VA 22908; [b]Department of Molecular, Cell and Cancer Biology, University of Massachusetts Medical School, Worcester, MA 01605; [c]Programs in Molecular Medicine and Bioinformatics and Integrative Biology, University of Massachusetts Medical School, Worcester, MA 01605; [d]Department of Neuroscience, University of Virginia School of Medicine, Charlottesville, VA 22908; and [e]Howard Hughes Medical Institute, University of Massachusetts Medical School, Worcester, MA 01605

Contributed by Michael R. Green, June 19, 2018 (sent for review March 2, 2018; reviewed by Aseem Z. Ansari and Sukesh R. Bhaumik)

Rett syndrome (RTT) is a genetic disorder resulting from a loss-of-function mutation in one copy of the X-linked gene methyl-CpG–binding protein 2 (*MECP2*). Typical RTT patients are females and, due to random X chromosome inactivation (XCI), ∼50% of cells express mutant MECP2 and the other ∼50% express wild-type MECP2. Cells expressing mutant MECP2 retain a wild-type copy of MECP2 on the inactive X chromosome (Xi), the reactivation of which represents a potential therapeutic approach for RTT. Previous studies have demonstrated reactivation of Xi-linked *MECP2* in cultured cells by biological or pharmacological inhibition of factors that promote XCI (called "XCI factors" or "XCIFs"). Whether XCIF inhibitors in living animals can reactivate Xi-linked *MECP2* in cerebral cortical neurons, the cell type most therapeutically relevant to RTT, remains to be determined. Here, we show that pharmacological inhibitors targeting XCIFs in the PI3K/AKT and bone morphogenetic protein signaling pathways reactivate Xi-linked *MECP2* in cultured mouse fibroblasts and human induced pluripotent stem cell-derived postmitotic RTT neurons. Notably, reactivation of Xi-linked *MECP2* corrects characteristic defects of human RTT neurons including reduced soma size and branch points. Most importantly, we show that intracerebroventricular injection of the XCIF inhibitors reactivates Xi-linked *Mecp2* in cerebral cortical neurons of adult living mice. In support of these pharmacological results, we also demonstrate genetic reactivation of Xi-linked *Mecp2* in cerebral cortical neurons of living mice bearing a homozygous XCIF deletion. Collectively, our results further establish the feasibility of pharmacological reactivation of Xi-linked *MECP2* as a therapeutic approach for RTT.

Mecp2 | mouse model | Rett syndrome | X chromosome reactivation | brain neurons

Rett syndrome (RTT) is a rare neurodevelopmental disease characterized by a constellation of features including epilepsy, autistic-like behaviors, and delayed development (1). Most RTT patients are females who carry a heterozygous loss-of-function mutation in an X-linked gene, *MECP2*, encoding methyl CpG-binding protein 2 (2). MECP2 is essential for proper neuronal morphology and synaptic function in the brain (3). Currently, there are no curative therapies for RTT, and the only treatments available are palliative.

Because *MECP2* is X-linked, its allele-specific expression pattern is determined by X chromosome inactivation (XCI), a mammalian dosage compensation mechanism in which one X chromosome is randomly epigenetically silenced and is referred to as the "inactive" X chromosome (Xi) (4). As a result of XCI, ∼50% of cells in RTT females carry a wild-type but silenced copy of *MECP2* on the Xi chromosome, which, if reactivated, can compensate for MECP2 deficiency. This approach has potential therapeutic relevance, as conditional expression of wild-type *Mecp2* in a mouse model of RTT is sufficient to rescue multiple disease features (5–7). In addition, the results of experiments in genetically engineered mouse models have shown that wild-type *Mecp2* is dominant in cells also expressing an *Mecp2* mutant (8).

Although Xi-linked *MECP2* reactivation has implications for the treatment of RTT, the approach has been hampered by a lack of complete understanding of the molecular mechanisms of XCI and the key regulators involved. Recently, however, several large-scale screens have identified factors involved in XCI and have yielded important mechanistic insights (9–11). For example, using a large-scale RNAi-based screening strategy, we previously identified 13 XCI factors (XCIFs) that include two druggable proteins involved in cell signaling: 3-phosphoinositide-dependent protein kinase 1 (PDPK1), a component of the PI3K/protein kinase B (AKT) signaling pathway, and activin A receptor type 1 (ACVR1), a component of the bone morphogenetic protein (BMP) signaling pathway (11). Inhibition of XCIFs, including PDPK1 and ACVR1, reactivates Xi-linked genes in cultured cells, indicating the therapeutic potential of these targets for treating X-linked diseases such as RTT. To date, however, pharmacological reactivation of Xi-linked genes such as *MECP2* has been demonstrated only in cultured cells, primarily in dividing cells such as mouse and human fibroblasts and differentiated embryonic stem cells (9–12). Whether reactivation of Xi-linked *MECP2* can occur in living animals in postmitotic brain neurons, the cell type most therapeutically relevant to RTT, remains to be determined.

Here, we show that small-molecule inhibitors of ACVR1 and downstream effectors of PDPK1 can reactivate Xi-linked *MECP2* in nondividing cultured RTT neurons and in cerebral cortical neurons of adult mice. These proof-of-concept results

Significance

Rett syndrome (RTT) is a devastating neurodevelopmental disorder with no cure. RTT typically affects females and is caused by mutations in one of the two copies of the X-linked gene *MECP2*. Due to X chromosome inactivation, the random silencing of one X chromosome, females with RTT have a mixture of cells that express either normal or mutant *MECP2*. Importantly, cells expressing mutant *MECP2* retain a normal copy of *MECP2* on the inactive X chromosome (Xi), the reactivation of which represents a potential therapeutic approach for RTT. Here we use small-molecule inhibitors to reactivate the Xi-linked *Mecp2* gene in brain neurons of living mice. Our results further establish the feasibility of Xi-linked *MECP2* reactivation-based therapeutics for treatment of RTT.

Author contributions: P.P., U.W., M.J.M., J.T.-S., and S.B. designed research; P.P., U.W., Z.Z., R.S., and S.B. performed research; M.R.G. contributed new reagents/analytic tools; P.P., J.Y., L.J.Z., J.T.-S., and S.B. analyzed data; and P.P., M.R.G., and S.B. wrote the paper.

Reviewers: A.Z.A., University of Wisconsin-Madison; and S.R.B., Southern Illinois University School of Medicine.

The authors declare no conflict of interest.

Published under the PNAS license.

[1]To whom correspondence may be addressed. Email: sb5fk@virginia.edu or michael.green@umassmed.edu.

This article contains supporting information online at www.pnas.org/lookup/suppl/doi:10.1073/pnas.1803792115/-/DCSupplemental.

Published online July 16, 2018.

help establish the feasibility of pharmacological reactivation of Xi-linked *MECP2* as a therapeutic approach for RTT.

Results

Pharmacological Inhibitors of ACVR1 Reactivate Xi-Linked *Mecp2*. We previously showed that shRNA-mediated knockdown of ACVR1 reactivates Xi-linked genes, including *MECP2* (11), and therefore sought to determine whether small-molecule inhibitors of ACVR1 could reproduce these effects. We treated female mouse fibroblast BMSL2 cells with an ACVR1 inhibitor (dorsomorphin, LDN193189 or K02288) or, as a control, with DMSO and analyzed the expression of *Mecp2* by RNA FISH. Cells treated with DMSO had, as expected, a single nuclear signal for *Mecp2*, indicative of monoallelic expression (Fig. 1*A*). Treatment with an ACVR1 inhibitor substantially increased the percentage of cells containing two nuclear *Mecp2* signals, indicating biallelic expression. We also tested the ACVR1 inhibitors in a second, unrelated female mouse fibroblast cell line, H4SV, which harbors a transgenic copy of *Gfp* on the Xi chromosome (Xi-*TgGfp*) (13). ACVR1 inhibitor treatment substantially increased the percentage of GFP^+ H4SV cells, indicating Xi-*TgGfp* reactivation (*SI Appendix*, Fig. S1*A*). We confirmed that each ACVR1 inhibitor efficiently inhibited BMP signaling (*SI Appendix*, Fig. S1*B*) and did not adversely affect cell survival (*SI Appendix*, Fig. S1*C*).

We and others have previously shown that XCIF inhibition leads to decreased levels of *Xist* (10, 11), a long noncoding RNA that coats the Xi chromosome in *cis* and mediates XCI (14). Consistent with these results, qRT-PCR analysis revealed that treatment of H4SV cells with either LDN193189 (Fig. 1*B*) or dorsomorphin (*SI Appendix*, Fig. S1*D*) resulted in a time-dependent decrease in *Xist* transcript levels. Interestingly, the decrease in *Xist* levels at 0–4 d following treatment with the ACVR1 inhibitor was followed by a large increase in Xi-*TgGfp* expression at 4–6 d, suggesting that the loss of *Xist* precedes Xi-linked gene reactivation. Removal of the ACVR1 inhibitor restored *Xist* expression to normal levels and was accompanied by silencing of Xi-*TgGfp* (Fig. 1*B* and *SI Appendix*, Fig. S1*D*), indicating that the ACVR1 inhibitors reversibly modulate Xi chromosome transcription.

Pharmacological Inhibitors of the PDPK1 Effectors mTOR and SGK1 Reactivate Xi-Linked *Mecp2*. We have previously demonstrated that small-molecule inhibitors of PDPK1, another XCIF identified in our original screen, reactivate the Xi-linked *Mecp2* gene (11). PDPK1 has multiple effector substrates, including mechanistic target of rapamycin kinase (mTOR), serum/glucocorticoid-regulated kinase 1 (SGK1), AKT, p70 ribosomal protein S6 kinase, PKC, and PKN (15). Inhibiting the downstream effectors of PDPK1 may result in more targeted reactivation of the Xi chromosome with less toxicity.

Of the PDPK1 effector substrates, we elected to focus on pharmacological inhibitors of mTOR and SGK1 because their therapeutic potential has been well demonstrated (16–19). Pharmacological inhibition of mTOR using the small-molecule inhibitor rapamycin, everolimus, or KU-0063794 substantially increased biallelic expression of *Mecp2* in BMSL2 cells (Fig. 1*C*) and reactivated Xi-*TgGfp* in H4SV cells (*SI Appendix*, Fig. S1*E*). Similarly, inhibition of SGK1 with either a small-molecule inhibitor (GSK650394) or an shRNA substantially increased biallelic expression of *Mecp2* in BMSL2 cells (Fig. 1*D* and *SI Appendix*, Fig. S1*F*) and reactivated Xi-*TgGfp* in H4SV cells (*SI Appendix*, Fig. S1*E*). As expected, the mTOR and SGK1 inhibitors inhibited their respective signaling pathways (*SI Appendix*, Fig. S1 *G* and *H*) and did not affect cell survival (*SI Appendix*, Fig. S1*I*).

Similar to the results with the ACVR1 inhibitors, there was a time-dependent decrease in *Xist* levels following treatment of H4SV cells with rapamycin or GSK650394, (Fig. 1 *E* and *F*). Consistent with the results shown in Fig. 1*B*, the reduction in *Xist* at 0–4 d following rapamycin or GSK650394 treatment was followed by a large increase in *Xi-TgGfp* expression at 4–6 d. Removal of rapamycin or GSK650394 restored normal levels of *Xist* and resulted in Xi-*TgGfp* silencing (Fig. 1 *E* and *F*), indicating that the reactivation of Xi-linked genes was reversible.

Pharmacological Inhibitors of ACVR1 or PDPK1 Effectors Decrease *Xist* Expression by Preventing Recruitment of Transcription Activators to the *Xist* Promoter. Pharmacological inhibitors of ACVR1 or PDPK1 effectors may decrease *Xist* levels by affecting either *Xist* RNA stability or *Xist* transcription. Treatment of H4SV cells with an ACVR1 inhibitor did not affect the half-life of *Xist* (*SI Appendix*, Fig. S2 *A* and *B*), suggesting that the decreased levels of *Xist* following ACVR1 inhibition were predominantly transcriptional. Previous studies have shown that, upon ligand engagement, ACVR1 activates receptor tyrosine kinase activity, leading to phosphorylation of receptor-regulated SMAD, which acts as a transcription factor in the nucleus (20). We identified putative SMAD-binding motifs in the *Xist* promoter and assessed the recruitment of phosphorylated SMAD to the *Xist* promoter by ChIP analysis in H4SV cells, which harbor a *Xist* deletion on the active X chromosome (Xa), enabling us to analyze binding of factors specifically to the Xi-linked *Xist* promoter. We found that

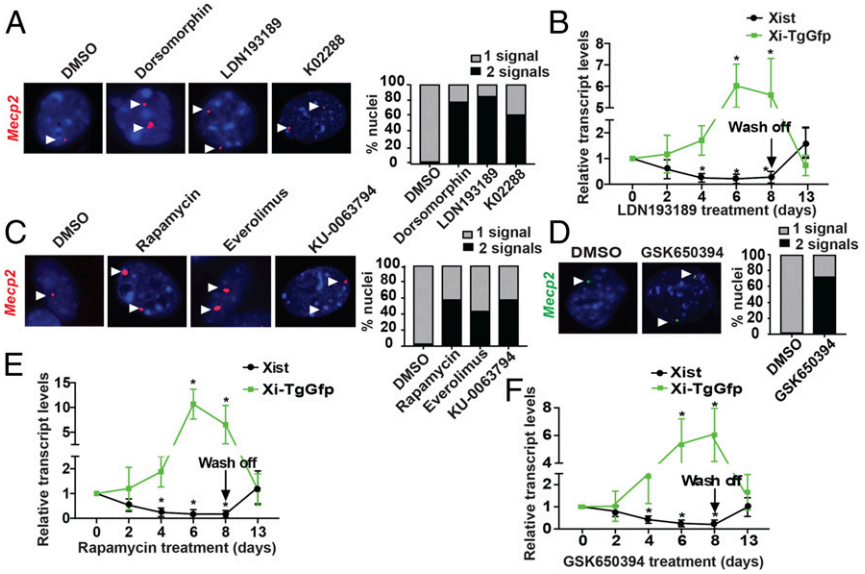

Fig. 1. Pharmacological inhibitors of the ACVR1 or PDPK1 effectors mTOR and SGK1 reactivate Xi-linked *Mecp2*. (*A*) RNA FISH monitoring of the expression of *Mecp2* (red) in BMSL2 cells treated with DMSO, dorsomorphin, LDN193189, or K02288. DAPI staining is shown in blue. Representative images are shown (*Left*) and the results are quantified (*Right*). (*B*) qRT-PCR monitoring of *Xist* (black) and Xi-*TgGfp* (green) expression in H4SV cells treated with LDN193189, 5 d following the removal of the inhibitor. The results were normalized to those obtained at day 0, which was set to 1. (*C* and *D*) RNA FISH monitoring of the expression of *Mecp2* in BMSL2 cells treated with DMSO, rapamycin, everolimus, or KU-0063794 (*C*) or GSK650394 (*D*). DAPI staining is shown in blue. Representative images are shown (*Left*), and the results are quantified (*Right*). (*E* and *F*) qRT-PCR monitoring *Xist* (black) and Xi-*TgGfp* (green) expression in H4SV cells treated with rapamycin (*E*) or GSK650394 (*F*), 5 d following the removal of the inhibitor. Error bars indicate SD; $*P < 0.05$.

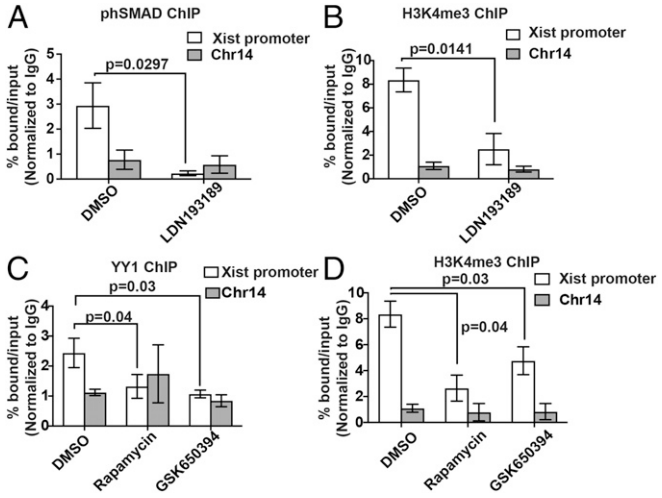

Fig. 2. Pharmacological inhibitors of ACVR1 or PDPK1 effectors decrease *Xist* expression by preventing the recruitment of transcription activators to the *Xist* promoter. (*A* and *B*) ChIP analysis monitoring the binding of phosphorylated SMAD (phSMAD) (*A*) and H3K4me3 (*B*) on the *Xist* promoter and a negative control region in chromosome 14 (Chr14) in H4SV cells treated with DMSO or LDN193189. (*C* and *D*) ChIP analysis monitoring the binding of YY1 (*C*) and H3K4me3 (*D*) on the *Xist* promoter and Chr14 region in H4SV cells treated with DMSO, rapamycin, or GSK650394. Error bars indicate SD.

phosphorylated SMAD was bound to the Xi-linked *Xist* promoter and was substantially decreased following treatment with LDN193189 (Fig. 2*A*) or dorsomorphin (*SI Appendix*, Fig. S2*C*). Furthermore, enrichment of the activating histone modification H3 lysine 4 trimethylation (H3K4me3), which is associated with the Xi-linked *Xist* promoter (21), was reduced following treatment with LDN193189 (Fig. 2*B*) or dorsomorphin (*SI Appendix*, Fig. S2*D*).

Similar to the results with ACVR1 inhibitors, an inhibitor of mTOR (rapamycin) or SGK1 (GSK650394) did not affect the half-life of *Xist* (*SI Appendix*, Fig. S2*E*). Previous studies have shown that *Xist* transcription is stimulated by recruitment of the transcription factor Ying-yang 1 (YY1), and ten YY1-binding sites have been identified in the *Xist* promoter (22). Consistent with these studies, we found that YY1 was bound to the Xi-linked *Xist* promoter and was significantly reduced by treatment with mTOR or SGK1 inhibitors (Fig. 2*C*). As expected, H3K4me3 enrichment on the *Xist* promoter was also significantly decreased following treatment with an mTOR or SGK1 inhibitor (Fig. 2*D*). Conversely, treatment with inhibitors of a PDPK1 effector and ACVR1 resulted in an enhancement of H3K4me3 and reduction of the repressive histone marks H2A ubiquitination (H2A-ub) and H3 lysine 27 trimethylation (H3K27me3) on an Xi-linked gene (*SI Appendix*, Fig. S2*F*). Notably, an ACVR1 inhibitor did not affect YY1 binding on the *Xist* promoter, and PDPK1 effector inhibitors did not affect SMAD binding (*SI Appendix*, Fig. S2*G*). Collectively, our results show that inhibition of ACVR1, mTOR, or SGK1 decreases the recruitment of a transcriptional activator to the Xi-linked *Xist* promoter, thereby decreasing *Xist* transcription and resulting in the reactivation of Xi-linked genes.

Synergistic Xi Chromosome Reactivation by Combined Inhibition of ACVR1 and a PDPK1 Effector. The results described above suggested the possibility of cooperativity between the PI3K/AKT and BMP signaling pathways in regulating Xi-linked *Xist* transcription. To interrogate synergy between the two pathways, we treated female mouse fibroblast cell lines with an inhibitor of ACVR1 (LDN193189) or a PDPK1 effector (rapamycin or GSK650394), either alone or in combination. BMSL2 cells contain an Xi-linked hypoxanthine-guanine phosphoribosyltransferase gene (*Hprt*), allowing reactivation of the Xi chromosome to be assayed by the survival of cells in hypoxanthine-aminopterin-thymidine (HAT) selection medium (13). Treatment of cells with LDN193189, rapamycin, or GSK650394 alone resulted in a modest increase in the number of colonies surviving in HAT selection medium (Fig. 3 *A* and *B*). By contrast, combined drug treatments—either LDN193189 and rapamycin or LDN193189 and GSK650394—synergistically increased the number of colonies surviving in HAT selection medium. Similarly, combined drug treatments synergistically increased the percentage of H4SV cells scoring as GFP$^+$ (Fig. 3*C* and *SI Appendix*, Fig. S3*A*). Importantly, the combined drug treatment did not adversely affect cellular proliferation (*SI Appendix*, Fig. S3*B*).

Pharmacological Reactivation of Xi-Linked *MECP2* in RTT Neurons Rescues Characteristic Morphological Defects. We next sought to investigate the efficacy of pharmacological XCIF inhibitors in reactivating Xi-linked wild-type *MECP2* in human postmitotic neurons, the cell type most relevant to RTT. To obtain RTT neurons, we used a previously described clonal induced pluripotent stem cell (iPSC) line, T158M-iPSC, which was derived from GM17880, an RTT fibroblast cell line that harbors a heterozygous T158M missense mutation in *MECP2* (23). The T158M-iPSC clone carries mutant *MECP2* on the Xa chromosome and wild-type *MECP2* on the Xi chromosome (23). As a positive isogenic control, we used a non-RTT iPSC clone, which was also derived from GM17880 but carries wild-type *MECP2* on the Xa. Neuronal differentiation was initiated to produce neuronal precursor cells, which were then differentiated into neurons (23, 24). RTT neurons were treated with either DMSO or the two drugs (LDN193189 and GSK650394) for 3 wk, and *MECP2* mRNA was monitored using Taqman probes specific for either wild-type or mutant *MECP2*. Drug treatment of RTT neurons resulted in increased expression of Xi-linked wild-type *MECP2* compared with that obtained with DMSO (Fig. 4*A*). Notably, the amount of Xi-linked *MECP2* expressed in drug-treated RTT neurons was ~10% of that observed in control neurons that express wild-type MECP2 from the Xa chromosome.

RTT patients have defective neuronal organization and dendritic complexity, including reduced glutamatergic synapse number, soma size, and number of dendritic spines (23). We

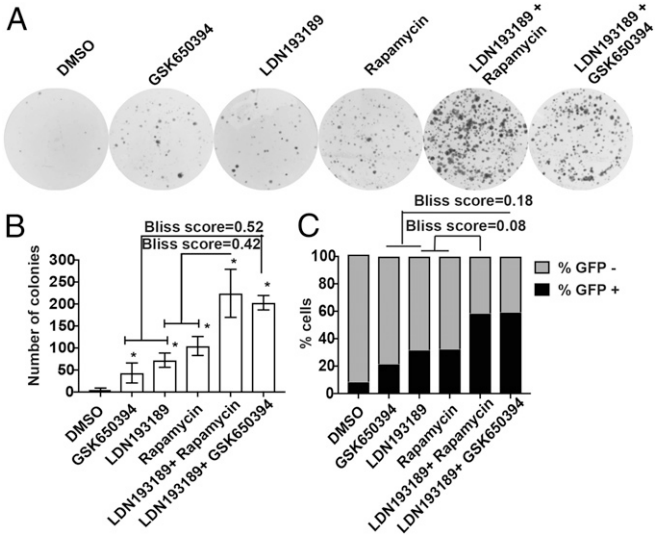

Fig. 3. Synergistic Xi chromosome reactivation by combined inhibition of ACVR1 and a PDPK1 effector. (*A*) Bright-field images showing the growth of BMSL2 cells treated with DMSO, GSK650394, LDN193189, or rapamycin either alone or in combination and followed by selection in HAT medium. (*B*) The colonies were quantified after crystal violet staining. Error bars indicate SD; *$P < 0.05$. (*C*) Quantification of GFP$^+$ H4SV cells treated with DMSO, GSK650394, LDN193189, or rapamycin either alone or in combination. A Bliss synergy score >0 indicates the synergistic effect of the drug combination.

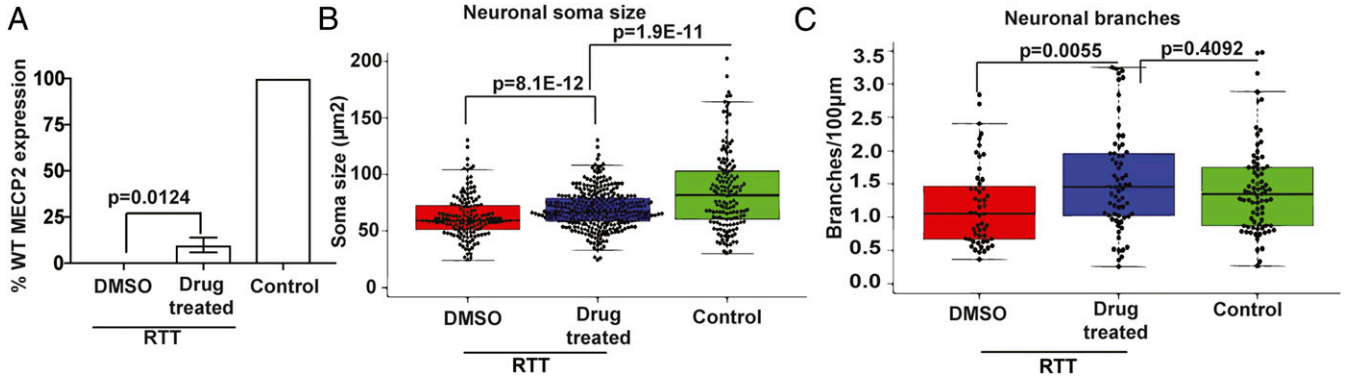

Fig. 4. Pharmacological reactivation of Xi-linked *MECP2* in RTT neurons rescues characteristic morphological defects. (*A*) qRT-PCR analysis monitoring the expression of Xi-linked wild-type *MECP2* in RTT neurons treated with DMSO or the combination of LDN193189 and GSK650394 (drug treated). Neurons derived from a clone expressing wild-type *MECP2* from the Xa were used as a positive control (Control), which was set to 100. (*B* and *C*) Quantitative analysis of the soma cross-sectional area (*B*) and the number of neuronal branch points (*C*) in MAP2$^+$ RTT neurons treated with DMSO or the drug combination. Neurons derived from a clone expressing wild-type *MECP2* from the Xa were used as a positive control. Each dot represents one neuron.

therefore asked whether pharmacological reactivation of Xi-linked wild-type *MECP2* could correct the morphological defects of RTT neurons. Drug treatment of MAP2$^+$ RTT neurons resulted in an increase in soma size (Fig. 4*B* and *SI Appendix*, Fig. S4*A*) and branch points (Fig. 4*C* and *SI Appendix*, Fig. S4*A*) compared with that obtained with DMSO. By contrast, drug

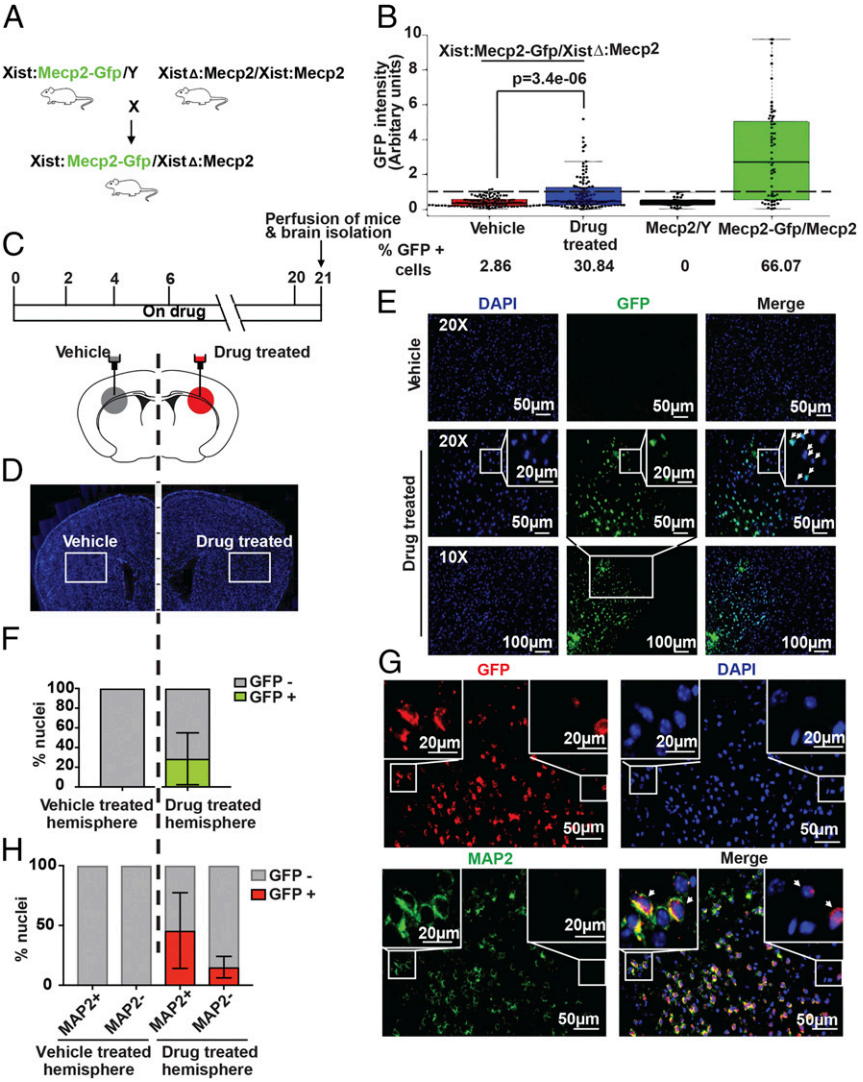

Fig. 5. Pharmacological reactivation of X-linked *Mecp2* in cerebral cortical neurons of living mice. (*A*) Schematic of the breeding strategy for generating *XistΔ:Mecp2/Xist:Mecp2-Gfp* mice. (*B*) Quantitative immunofluorescence monitoring GFP intensity in female *XistΔ:Mecp2/Xist:Mecp2-Gfp* MEFs following treatment with DMSO or the drugs LDN193189 and GSK650394. MEFs isolated from *Mecp2/Y* or *Mecp2/Mecp2-Gfp* mice were used as negative and positive controls, respectively. Each dot represents a MEF, and a dashed line indicates the maximum background signal obtained in *Mecp2/Y*, which was set to 1. (*C*, *Upper*) Schematic of the drug regimen. (*Lower*) Schematic of a mouse brain showing the site of injection for vehicle or drug in the left or right hemisphere of the brain. (*D*) Representative immunofluorescence images of the coronal brain sections from female *XistΔ:Mecp2/Xist:Mecp2-Gfp* mice injected with vehicle or drug. The site of injection is represented by the white box. DAPI staining is shown in blue. (*E*) Representative immunofluorescence images showing endogenous GFP signal (green) in coronal brain sections from vehicle- or drug-treated hemispheres (n = 4). DAPI staining is shown in blue. (*F*) Quantitation of GFP$^+$ nuclei in four hemispheres. (*G*) Representative immunofluorescence images of the coronal brain sections monitoring the expression of GFP (anti-GFP; red) and MAP2 (green) in vehicle- and drug-treated hemispheres (n = 4). DAPI staining is shown in blue. (*H*) Quantitation of GFP$^+$ nuclei in MAP2$^+$ and MAP2$^-$ cells in vehicle- and drug-treated hemispheres (n = 4). Error bars indicate SD.

treatment had no effect on control neurons (*SI Appendix*, Fig. S4 *B* and *C*). Thus, our results demonstrate that pharmacological reactivation of Xi-linked *MECP2* can correct characteristic neuronal morphological defects of RTT neurons.

Pharmacological Reactivation of Xi-Linked *Mecp2* in Cerebral Cortical Neurons of Living Mice. We next sought to determine whether pharmacological XCIF inhibitors could reactivate Xi-linked *Mecp2* in the brain of an adult mouse. Toward this end, we used a *Xist**Δ**:Mecp2/Xist:Mecp2-Gfp* mouse model harboring an Xi-linked *Mecp2-Gfp* reporter (Fig. 5*A* and *SI Appendix*, Fig. S5*A*), which allows accurate and robust quantitation of Xi-linked *Mecp2* reactivation because (*i*) 100% of cells carry *Mecp2-Gfp* on the Xi chromosome, and thus the results are not confounded by variable mosaic expression of GFP in different animals, and (*ii*) the genetic labeling of endogenous *Mecp2* permits direct visualization of individual neurons with reactivated *Gfp*, thereby minimizing the experimental manipulations required for analysis of Xi-linked *Mecp2* reactivation.

To assess the feasibility of the *XistΔ:Mecp2/Xist:Mecp2-Gfp* mouse model for monitoring Xi-linked *Mecp2* reactivation, we first treated mouse embryonic fibroblasts (MEFs) isolated from female D15.5 *Xist**Δ**:Mecp2/Xist:Mecp2-Gfp* embryos with either DMSO or the two drugs LDN193189 and GSK650394. Drug treatment, but not DMSO, reactivated expression of Xi-*Mecp2-Gfp* (*SI Appendix*, Fig. S5*B*). Immunoblot analysis confirmed the inhibition of BMP and PI3K/AKT pathways in drug-treated MEFs (*SI Appendix*, Fig. S5*C*).

To determine the extent of Xi-*Mecp2-Gfp* expression in individual MEFs, we carried out quantitative immunofluorescence. Negative-control MEFs isolated from male embryos (*Mecp2/Y*) had no detectable GFP, whereas ∼66% of positive-control *Mecp2-Gfp/Mecp2* MEFs had a nuclear GFP signal (Fig. 5*B*). As expected, *XistΔ:Mecp2/Xist:Mecp2-Gfp* MEFs treated with DMSO had a very low level of nuclear GFP (∼3%). By contrast, ∼31% of drug-treated *XistΔ:Mecp2/Xist:Mecp2* MEFs were positive for nuclear GFP. Quantitative analysis of fluorescence signals revealed variable fluorescence intensity in GFP$^+$ MEFs, which likely reflects heterogeneous expression levels in different cells, consistent with a previous report (25).

Next, we tested whether the drug treatment could reactivate Xi-linked *Mecp2* in the brain of *Xist**Δ**:Mecp2/Xist:Mecp2-Gfp* female mice. We administered vehicle or the two drugs in opposite brain hemispheres of 4-wk-old *Xist**Δ**:Mecp2/Xist:Mecp2-Gfp* female mice by intracerebroventricular injection using stereotactic surgical procedures (Fig. 5 *C* and *D*). Three weeks later, a subset of animals was killed, and the expression of wild-type *Mecp2* and Xi-*Mecp2-Gfp* in the vehicle- and drug-infused hemispheres was determined by RT-PCR, which revealed that wild-type *Mecp2* expression was detected in both the vehicle- and drug-infused hemispheres but the Xi-*Mecp2-Gfp* transcript was detected only in the drug-infused hemisphere (*SI Appendix*, Fig. S5*D*). Immunofluorescence analysis of coronal brain sections showed that after 3 wk there was reactivation of Xi-Mecp2-Gfp in ∼30% of cells in the drug-infused hemisphere, whereas Xi-Mecp2-Gfp was not detected in the vehicle-infused hemisphere (Fig. 5 *E* and *F* and *SI Appendix*, Fig. S5*E*). Consistent with previous results (11, 26), total levels of *Mecp2* were not increased following drug treatment (*Discussion* and *SI Appendix*, Fig. S5*F*).

Finally, we assessed the extent of Xi-*Mecp2-Gfp* reactivation specifically in cerebral cortical neurons. Double immunostaining of coronal brain sections from drug-infused hemispheres showed that a large number of MAP2$^+$ neurons were also GFP$^+$, indicative of *Xi-Mecp2-Gfp* expression (Fig. 5*G*). Specifically, in the drug-infused hemisphere ∼45% of MAP2$^+$ and ∼20% of MAP2$^-$ brain cells expressed GFP, confirming Xi-*Mecp2-Gfp* reactivation in cerebral cortical neurons as well as in nonneuronal cells (Fig. 5*H*). Immunoblot analysis confirmed the inhibition of BMP and PI3K/AKT pathways in the brain (*SI Appendix*, Fig. S5*G*) but, as expected, not in the liver (*SI Appendix*, Fig. S5*H*). There was no significant change in the body weight of drug-treated mice over the duration of the experiment (*SI Appendix*, Fig. S5*I*).

Genetic Reactivation of Xi-Linked *Mecp2* in Living Mice. To complement the results of our pharmacological reactivation experiments, we sought to determine whether Xi-linked *Mecp2* reactivation could be achieved genetically. Stanniocalcin 1 (STC1), another XCIF identified in our previous RNAi screen (11), is a ubiquitous glycoprotein whose function is poorly understood (27). *Stc1*$^{-/-}$ mice have no obvious phenotype (28), and we have previously shown that loss of *Stc1* results in biallelic expression of X-linked genes, including *Mecp2* (11).

We generated *Stc1*$^{-/-}$*:Mecp2/Mecp2-Gfp*, *Stc1*$^{+/-}$*:Mecp2/Mecp2-Gfp* and *Stc1*$^{+/+}$*:Mecp2/Mecp2-Gfp* mice (*SI Appendix*, Fig. S6*A*) in which at least half of all cells were expected to carry *Mecp2-Gfp* on the Xi chromosome. The genotype of the littermates was confirmed by PCR (*SI Appendix*, Fig. S6*B*). We then asked if genetic loss of *Stc1* reactivates the *Mecp2-Gfp* reporter on the Xi chromosome, thereby increasing the number of GFP$^+$ brain cells in *Stc1*$^{-/-}$*:Mecp2/Mecp2-Gfp* mice compared with *Stc1*$^{+/+}$*:Mecp2/Mecp2-Gfp* mice. Nuclei from the mouse brain cells were isolated and analyzed by FACS for GFP (*SI Appendix*, Fig. S6*C*). As expected, GFP$^+$ brain nuclei from *Mecp2*$^{+/+}$ mice were undetectable, whereas 100% of brain nuclei from *Mecp2-Gfp/Mecp2-Gfp* mice were GFP$^+$ (Fig. 6*B*). Nuclei isolated from mouse brains were sorted into neuronal and nonneuronal populations based on the expression of the neuronal nuclear marker NeuN. Consistent with our previous results (11), genetic loss of *Stc1* led to a significant increase in the percentage of GFP$^+$ nuclei in both NeuN$^+$, and NeuN$^-$ brain cells, indicating Xi-linked *Mecp2* reactivation (Fig. 6 *A* and *B*).

Next, to analyze these results in genetically and environmentally comparable backgrounds, we compared the percentage of GFP$^+$ nuclei in *Stc1*$^{-/-}$*:Mecp2/Mecp2-Gfp* and *Stc1*$^{+/+}$*:Mecp2/Mecp2-Gfp* littermates. Strikingly, the increase in GFP$^+$ brain cells was more pronounced when the comparison was between littermates (Fig. 6 *C* and *D*), which may be due to a 65:35 skewing of XCI in the brain cells of *Mecp2/Mecp2-Gfp* mice (*SI Appendix*, Fig. S6*D*) as described for the human population (29). In summary, these results show that Xi-linked *Mecp2* can be reactivated in a mouse brain by genetic manipulation of an XCIF.

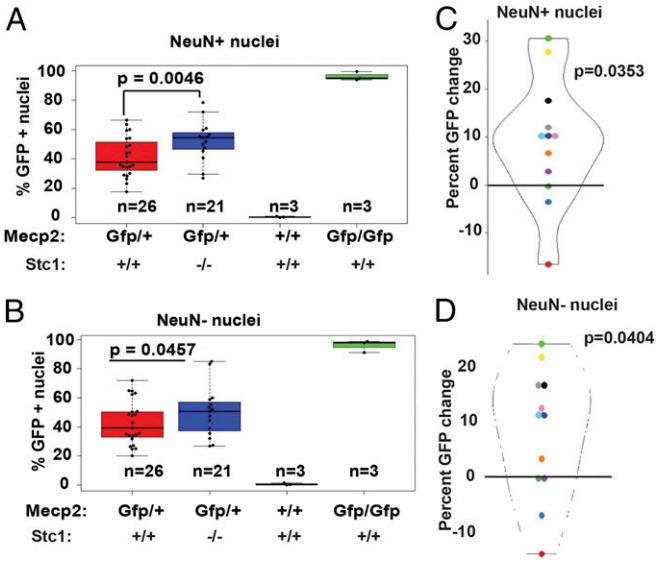

Fig. 6. Genetic reactivation of Xi-linked *Mecp2* in living mice. (*A* and *B*) Boxplots of percent GFP$^+$ NeuN$^+$ (*A*) and NeuN$^-$ (*B*) nuclei isolated from the brain cells of mice. Error bars indicate SD. (*C* and *D*) Violin plots showing the percent change in GFP$^+$ NeuN$^+$ (*C*) and NeuN$^-$ (*D*) nuclei in the brains of *Stc1*$^{-/-}$*:Mecp2/Mecp2-Gfp* mice compared with *Stc1*$^{+/+}$*:Mecp2/Mecp2-Gfp* littermates. Each dot represents the percent change in the GFP$^+$ population within a litter (n = 12).

Discussion

Pharmacological inhibition of XCIFs represents a strategy to reactivate the Xi-linked *MECP2* gene as a therapeutic approach for RTT. In this study, we showed that pharmacological inhibitors of XCIFs, in particular the ACVR1 and PDPK1 effectors mTOR and SGK1, reactivate the Xi-linked *Mecp2* gene in mouse fibroblasts, human RTT neurons, and, most importantly, cerebral cortical neurons of adult living mice. Our results provide an important proof of concept for the feasibility of reactivating Xi-linked *MECP2* as a treatment for RTT. Notably, the mTOR inhibitors in our study are currently used to prevent transplant rejection and are being investigated as therapeutics for cancer and neurodegenerative diseases (30–32).

A potential concern for a therapy based on Xi chromosome reactivation is that the increase in X-linked gene expression may be deleterious. However, several lines of evidence indicate the existence of a compensatory mechanism that prevents increased total X-linked gene expression in cells with defective XCI. For example, transcriptome profiling studies have shown that the XCI defect observed in *Stc1*$^{-/-}$ mice is not accompanied by changes in expression of the majority (98%) of X-linked genes (11). Similarly, *Xist* deletion in mouse hematopoietic cells has been shown to result in changes in only ∼2–12% of X-linked genes (11, 26). Furthermore, a recent study analyzing the effect of *Xist* deletion in mice revealed that the X:autosomal gene balance was not significantly altered despite the increase in the expression of X-linked genes (33). Collectively, these studies indicate that reactivation of the Xi chromosome will not increase the total expression levels of X-linked genes.

An attractive feature of an Xi-linked *MECP2* reactivation therapy is that it is based on correcting the root cause of the disease, the lack of wild-type *MECP2*, rather than some secondary, downstream consequence of the *MECP2* deficiency. In addition to RTT, there are several other diseases for which reactivation of an Xi-linked gene represents a potential therapeutic approach. For example, CDKL5 deficiency is a rare genetic disorder caused by mutations in the X-linked *CDKL5* gene (34). Similar to RTT, most patients with CDKL5 deficiency are female *CDKL5* heterozygotes, and reactivation of the Xi-linked *CDKL5* gene could have potential clinical benefit. Thus, the results described in this study have therapeutic implications for CDKL5 deficiency and other dominant X-linked monogenic disorders.

Materials and Methods

Materials and methods used for cell culture, mice, drug treatment, mouse cortex dissection, flow cytometry, RNAi, qRT-PCR, immunoblotting, immunofluorescence, RNA-FISH assay, ChIP assays, neuronal morphological analysis, the 3-[4,5-dimethylthiazol-2-yl]-2,5-diphenyltetrazolium bromide (MTT) assay, and in vivo drug treatment are available in *SI Appendix*. All quantitative data were collected from experiments performed at least in triplicate and are expressed as mean ± SD. Work involving mice adhered to the guidelines of the University of Virginia Institutional Animal Care and Use Committee (IACUC), protocol number 4112.

ACKNOWLEDGMENTS. We thank David Sheikh-Hamad, Antonio Bedalov, Maria C. N. Marchetto, and Fred H. Gage for providing reagents; the University of Virginia DNA Sciences Core for high-throughput sequencing; the University of Virginia Flow Cytometry Facility for FACS; the University of Virginia Tissue Histology Core for cryosectioning; Christian Blue and Saloni Singh for technical assistance with genotyping; and Sara Deibler for editorial assistance. M.R.G. is an investigator of the Howard Hughes Medical Institute. This work was supported by a Double Hoo Research Grant from the Office of Undergraduate Research at the University of Virginia (to Z.Z.); grants from the Rett Syndrome Research Trust and CDKL5 Program of Excellence funded by the LouLou Foundation and the Orphan Disease Center of the University of Pennsylvania (to M.R.G.); and a Pilot Project Program Award from the University of Virginia-Virginia Tech Seed Fund Award and The Hartwell Foundation Individual Biomedical Research Award (to S.B.).

1. Hagberg B (2002) Clinical manifestations and stages of Rett syndrome. *Ment Retard Dev Disabil Res Rev* 8:61–65.
2. Amir RE, et al. (2000) Influence of mutation type and X chromosome inactivation on Rett syndrome phenotypes. *Ann Neurol* 47:670–679.
3. Fasolino M, Zhou Z (2017) The crucial role of DNA methylation and MeCP2 in neuronal function. *Genes (Basel)* 8:E141.
4. Lyon MF (1971) Possible mechanisms of X chromosome inactivation. *Nat New Biol* 232: 229–232.
5. Garg SK, et al. (2013) Systemic delivery of MeCP2 rescues behavioral and cellular deficits in female mouse models of Rett syndrome. *J Neurosci* 33:13612–13620.
6. Sztainberg Y, et al. (2015) Reversal of phenotypes in MECP2 duplication mice using genetic rescue or antisense oligonucleotides. *Nature* 528:123–126.
7. Ure K, et al. (2016) Restoration of Mecp2 expression in GABAergic neurons is sufficient to rescue multiple disease features in a mouse model of Rett syndrome. *eLife* 5: e14198.
8. Heckman LD, Chahrour MH, Zoghbi HY (2014) Rett-causing mutations reveal two domains critical for MeCP2 function and for toxicity in MECP2 duplication syndrome mice. *eLife* 3:e02676.
9. Lessing D, et al. (2016) A high-throughput small molecule screen identifies synergism between DNA methylation and Aurora kinase pathways for X reactivation. *Proc Natl Acad Sci USA* 113:14366–14371.
10. Sripathy S, et al. (2017) Screen for reactivation of MeCP2 on the inactive X chromosome identifies the BMP/TGF-β superfamily as a regulator of XIST expression. *Proc Natl Acad Sci USA* 114:1619–1624.
11. Bhatnagar S, et al. (2014) Genetic and pharmacological reactivation of the mammalian inactive X chromosome. *Proc Natl Acad Sci USA* 111:12591–12598.
12. Carrette LLG, et al. (2018) A mixed modality approach towards Xi reactivation for Rett syndrome and other X-linked disorders. *Proc Natl Acad Sci USA* 115:E668–E675.
13. Komura J-i, Sheardown SA, Brockdorff N, Singer-Sam J, Riggs AD (1997) In vivo ultraviolet and dimethyl sulfate footprinting of the 5′ region of the expressed and silent Xist alleles. *J Biol Chem* 272:10975–10980.
14. Plath K, Mlynarczyk-Evans S, Nusinow DA, Panning B (2002) Xist RNA and the mechanism of X chromosome inactivation. *Annu Rev Genet* 36:233–278.
15. Bayascas JR (2010) PDK1: The major transducer of PI 3-kinase actions. *Curr Top Microbiol Immunol* 346:9–29.
16. Sherk AB, et al. (2008) Development of a small-molecule serum- and glucocorticoid-regulated kinase-1 antagonist and its evaluation as a prostate cancer therapeutic. *Cancer Res* 68:7475–7483.
17. Liang X, et al. (2017) Development of a new analog of SGK1 inhibitor and its evaluation as a therapeutic molecule of colorectal cancer. *J Cancer* 8:2256–2262.
18. Ellard SL, et al. (2009) Randomized phase II study comparing two schedules of everolimus in patients with recurrent/metastatic breast cancer: NCIC Clinical Trials Group IND.163. *J Clin Oncol* 27:4536–4541.
19. Wahl M, et al. (2017) Probing the phosphatidylinositol 3-kinase/mammalian target of rapamycin pathway in gliomas: A phase 2 study of everolimus for recurrent adult low-grade gliomas. *Cancer* 123:4631–4639.
20. von Bubnoff A, Cho KW (2001) Intracellular BMP signaling regulation in vertebrates: Pathway or network? *Dev Biol* 239:1–14.
21. Goto Y, Gomez M, Brockdorff N, Feil R (2002) Differential patterns of histone methylation and acetylation distinguish active and repressed alleles at X-linked genes. *Cytogenet Genome Res* 99:66–74.
22. Makhlouf M, et al. (2014) A prominent and conserved role for YY1 in Xist transcriptional activation. *Nat Commun* 5:4878.
23. Marchetto MC, et al. (2010) A model for neural development and treatment of Rett syndrome using human induced pluripotent stem cells. *Cell* 143:527–539.
24. McConnell MJ, et al. (2013) Mosaic copy number variation in human neurons. *Science* 342:632–637.
25. LaSalle JM, Goldstine J, Balmer D, Greco CM (2001) Quantitative localization of heterogeneous methyl-CpG-binding protein 2 (MeCP2) expression phenotypes in normal and Rett syndrome brain by laser scanning cytometry. *Hum Mol Genet* 10:1729–1740.
26. Yildirim E, et al. (2013) Xist RNA is a potent suppressor of hematologic cancer in mice. *Cell* 152:727–742.
27. Yeung BH, Law AY, Wong CK (2012) Evolution and roles of stanniocalcin. *Mol Cell Endocrinol* 349:272–280.
28. Chang AC, Cha J, Koentgen F, Reddel RR (2005) The murine stanniocalcin 1 gene is not essential for growth and development. *Mol Cell Biol* 25:10604–10610.
29. Tukiainen T, et al.; GTEx Consortium; Laboratory, Data Analysis &Coordinating Center (LDACC)—Analysis Working Group; Statistical Methods groups—Analysis Working Group; Enhancing GTEx (eGTEx) groups; NIH Common Fund; NIH/NCI; NIH/NHGRI; NIH/NIMH; NIH/NIDA; Biospecimen Collection Source Site—NDRI; Biospecimen Collection Source Site—RPCI; Biospecimen Core Resource—VARI; Brain Bank Repository—University of Miami Brain Endowment Bank; Leidos Biomedical—Project Management; ELSI Study; Genome Browser Data Integration &Visualization—EBI; Genome Browser Data Integration &Visualization—UCSC Genomics Institute, University of California Santa Cruz (2017) Landscape of X chromosome inactivation across human tissues. *Nature* 550: 244–248.
30. Chong ZZ, Shang YC, Wang S, Maiese K (2012) Shedding new light on neurodegenerative diseases through the mammalian target of rapamycin. *Prog Neurobiol* 99:128–148.
31. Wong M (2013) Mammalian target of rapamycin (mTOR) pathways in neurological diseases. *Biomed J* 36:40–50.
32. Johnson SC, et al. (2013) mTOR inhibition alleviates mitochondrial disease in a mouse model of Leigh syndrome. *Science* 342:1524–1528.
33. Yang L, Kirby JE, Sunwoo H, Lee JT (2016) Female mice lacking Xist RNA show partial dosage compensation and survive to term. *Genes Dev* 30:1747–1760.
34. Weaving LS, et al. (2004) Mutations of CDKL5 cause a severe neurodevelopmental disorder with infantile spasms and mental retardation. *Am J Hum Genet* 75:1079–1093.